

RESEARCH ARTICLE

Effects of PI(4,5)P₂ concentration on the F-BAR domain membrane binding as revealed by coarse-grained simulations

Tatiana B. Stanishneva-Konovalova  | Olga S. Sokolova 

Department of Bioengineering, Faculty of Biology, Lomonosov Moscow State University, Moscow, Russia

Correspondence

Tatiana B. Stanishneva-Konovalova, Department of Bioengineering, Faculty of Biology, Lomonosov Moscow State University, 1-12 Leninskie Gory, Moscow 119234, Russia. Email: sokolova@mail.bio.msu.ru

Funding information

Russian Foundation for Basic Research, Grant/Award Number: 18-34-00347

Abstract

Bin/Amphiphysin/Rvs (BAR) domain proteins form a key link between membrane remodeling and cytoskeleton dynamics. They are dimers that bind to membranes via electrostatic interactions with different preferences toward negatively charged lipids. In the present article, we examine the interactions of the F-BAR domain of nervous wreck (Nwk) with phosphatidylinositol 4,5-bisphosphate (PI(4,5)P₂)-containing membranes using coarse-grained molecular dynamics. We demonstrated PI(4,5)P₂ concentration effects, identified the sequence of events that underlies the protein binding and identified amino acids involved in protein–lipid interactions. Our simulations point out the primary role of the basic stretch at the tips of the dimer, which anchors the protein to the membrane and initiates the binding process. When the PI(4,5)P₂ concentration is high, the protein stably associates with the membrane by its concave surface or by the opposite side. At low PI(4,5)P₂ concentration, the former orientation becomes more favorable; also a state with only one tip bound is observed, due to the weaker attachment and more pronounced association/dissociation events. Our results provide a theoretical model that describes the lipid-binding behavior of Nwk observed in vitro.

KEYWORDS

lipid–protein interactions, molecular dynamics, negatively charged lipids, Nwk

1 | INTRODUCTION

Many cellular processes in eukaryotes imply the remodeling of the plasma membrane and often require the activities of BAR (Bin/Amphiphysin/Rvs) domain proteins. These proteins consist of a membrane-binding module, the BAR domain, and additional domains which control the cellular functions. BAR domains form crescent-shaped or zeppelin-shaped dimers with positively charged amino acid clusters which can bind to negatively charged lipids. When added to liposomes or expressed in cells, they often cause the formation of membrane tubules whose curvature and direction correlates with the structure of an individual domain.^{1–4} Large-scale membrane remodeling implies cooperative action of multiple BAR domain proteins.^{5,6}

Lipid preferences vary among different BAR domains, but many of them induce phosphoinositide clustering through electrostatic interactions.^{7,8} The most common phosphoinositide in the inner leaflet of the

plasma membrane is phosphatidylinositol 4,5-bisphosphate (PI(4,5)P₂).⁹ Interactions between PI(4,5)P₂ and BAR domains play important roles in various cellular processes: PI(4,5)P₂ clustering by the N-BAR domain of BIN1/M-Amphiphysin2 is essential for dynamin recruitment,⁸ srGAP3 is targeted to a specific part of the filopodial protrusions through its ability to preferentially bind PI(4,5)P₂,¹⁰ syndapin colocalizes with PI(4,5)P₂ at the cleavage furrow and interacts with the contractile ring component during cytokinesis.¹¹

Nwk functions in the *Drosophila* neuromuscular junction and contains one F-BAR and two SH3 domains that modulate the F-BAR's activity and are also responsible for interactions with WASp and other proteins engaged in actin dynamics.¹² In contrast to other F-BAR domains, the F-BAR domain of Nwk does not tubulate membranes of liposomes, but causes the formation of ridges and scallops.¹³ When expressed in cells, it induces extensive protrusion generation. A similar activity was observed for Nwk's mammalian homolog FCHSD2.¹⁴ In co-sedimentation analysis, the F-BAR of Nwk did not display a strong specificity for any particular phospholipid, but was preferably binding to more charged membranes, that either contained a high concentration of phosphatidylserine (~50%) or a low concentration of highly

Abbreviations: BAR, Bin/Amphiphysin/Rvs; DPPC, dipalmitoyl phosphatidylcholine; DPPI, dipalmitoyl phosphatidylinositol 4,5-bisphosphate; NCBI, National Center for Biotechnology Information; Nwk, Nervous wreck; PH, Pleckstrin Homology; PI(4,5)P₂, phosphatidylinositol-4,5-bisphosphate.

charged phosphoinositides (5%).¹³ In vitro, F-BAR domain binding to giant unilamellar vesicles demonstrated that, although higher membrane charge promotes membrane binding, it also impedes membrane deformation.¹⁵ Here, we develop a theoretical model that describes the lipid-binding behavior of Nwk's F-BAR domain at different PI(4,5)P₂ concentrations.

2 | METHODS

2.1 | Protein model

Due to the absence of crystal or high-resolution cryo-electron microscopy structures of the Nwk F-BAR domain, we used a homology-based method to build the protein model. Although the homology-based structure may miss the exact curvature of the F-BAR dimer, which is important for its membrane-shaping activity, it may serve as a useful tool to study protein–lipid interactions when the membrane curvature is not generated (ie, when a single dimer binds to a large patch of the planar lipid bilayer). The sequence of *Drosophila melanogaster* Nwk was obtained from the NCBI (accession number: AFH04360.1). The structure of the F-BAR domain of FBP17 (PDB code: 2EFL) was used as a template to build a model of Nwk's F-BAR domain (amino acids 16–281). Identification of the structural template, sequence alignment and model building were done in SWISS.¹⁶ Since all biochemical studies were performed on a fragment longer than the F-BAR domain alone, we also modeled an N-terminal peptide and a C-terminal α -helix adjacent to the F-BAR domain using a PEP-FOLD server for de novo peptide structure prediction.¹⁷ The final structure corresponded to fragment Nwk^{1–288}. UCSF Chimera¹⁸ was used to construct a dimer from the predicted structure by aligning it against the structure of dimerized FBP17 (Supporting Information Figure S1). Using the *martinize.py* script,¹⁹ the atomic structure was converted to an ELNEDIN (combined Elastic Network–coarse grained)²⁰ protein model. The protein was solvated in polarizable water with 0.15 M salt concentration, minimized, and equilibrated for 1 ns.

2.2 | Lipid models

In order to investigate the influence of PI(4,5)P₂ concentration on F-BAR domain binding we created membrane models with dipalmitoyl phosphatidylcholine (DPPC) as the major component and dipalmitoyl phosphatidylinositol 4,5-bisphosphate (DPPI) as the minor component at two concentrations: 3% and 10%. DPPC topology was taken from Martini 2.0 force field distribution.²¹ DPPI topology (Supporting Information) was based on the topology of PI(3,4)P₂ described earlier.²²

2.3 | Simulated systems

Using the *insane.py* script²³ we built 12 systems with a protein positioned 7 nm above the DPPI-containing leaflet (corresponding to the inner part of the plasma membrane). The distance between the protein and the membrane was chosen to prevent the protein from binding in an imposed orientation. In the first six systems, the upper leaflet was comprised of 1552 (97%) DPPC and 48 (3%) DPPI, in the next six systems, the upper leaflet consisted of 1440 (90%) DPPC and

160 (10%) DPPI. All opposite leaflets contained 1600 DPPC. For each DPPI concentration, we considered three initial protein orientations. Systems where the concave surface of the dimer was facing the membrane were denoted as X-top and X-top', where X is DPPI concentration. Similarly, systems where the protein was rotated 90° around the long axis were named X-side and X-side' and systems where the concave surface was facing away from the membrane were named X-bottom and X-bottom'. Note that systems with the same DPPI concentration and initial protein orientation were not identical, because they had different DPPI distributions in the upper leaflet. Initial dimensions of each system were 31 × 31 × 25 nm³; all systems were solvated in ~155 000 coarse-grained water molecules, ions were added to neutralize the system and reach 0.15 M concentration.

2.4 | MD protocols

All systems were energy minimized to reach $F_{\max} < 500$ and equilibrated for 1 ns. Simulation parameters were as described in²⁴ (parameter set “new”). Lennard-Jones and Coulomb interactions were treated using cut-off distances of 1.1 nm in combination with potential modifiers. The neighbor list was updated using the Verlet neighbor search algorithm. The particle Mesh Ewald algorithm was used for long-range electrostatic interactions.²⁵ The temperature was controlled with the velocity rescale thermostat²⁶ with a coupling parameter of 1.0 and a reference temperature of 323 K. The pressure of 1 bar was controlled semi-isotropically using the Berendsen algorithm²⁷ for equilibration and Parrinello-Rahman²⁸ for the production run with coupling parameter of 12.0 ps⁻¹. A time-step of 20 fs was used; systems with 10% DPPI were simulated for 1.5 μ s and systems with 3% DPPI for 2 μ s. Simulations were carried out in GROMACS-5.0.4-gpu with a Martini 2.2P force field¹⁹ and a polarizable water model. All calculations were performed on the “Lomonosov” supercomputer at Lomonosov Moscow State University.²⁹

2.5 | Data analysis

Lipid diffusion coefficients were calculated from an Einstein relation:

$$\text{MSD} = 4 \times 2d \times D_{\text{lat}} \times t$$

where MSD is the mean square displacement, d is the dimensionality of the systems ($d = 2$ because of the two-dimensional [2D] membrane) and a conversion factor of 4 was added in order to account for the acceleration of dynamics observed in coarse-grained models, as suggested by Marrink et al.³⁰ MSD was calculated using the *g_msd* tool in GROMACS.

Distances between centers of mass were calculated using the *distance* command; for protein-membrane contacts we used the *g_contact* program.³¹

To investigate the orientation of the F-BAR domain relative to the lipid bilayer, we applied an approach described in Ref. 32. We calculated normalized 2D histograms of R_{zz} and d_z values: R_{zz} is the zz component of the rotational matrix required for least squares fitting of a conformation onto a reference conformation, and d_z is the perpendicular distance between the centers of mass of the F-BAR domain and the lipid bilayer. R_{zz} was calculated using the *g_rotmat*

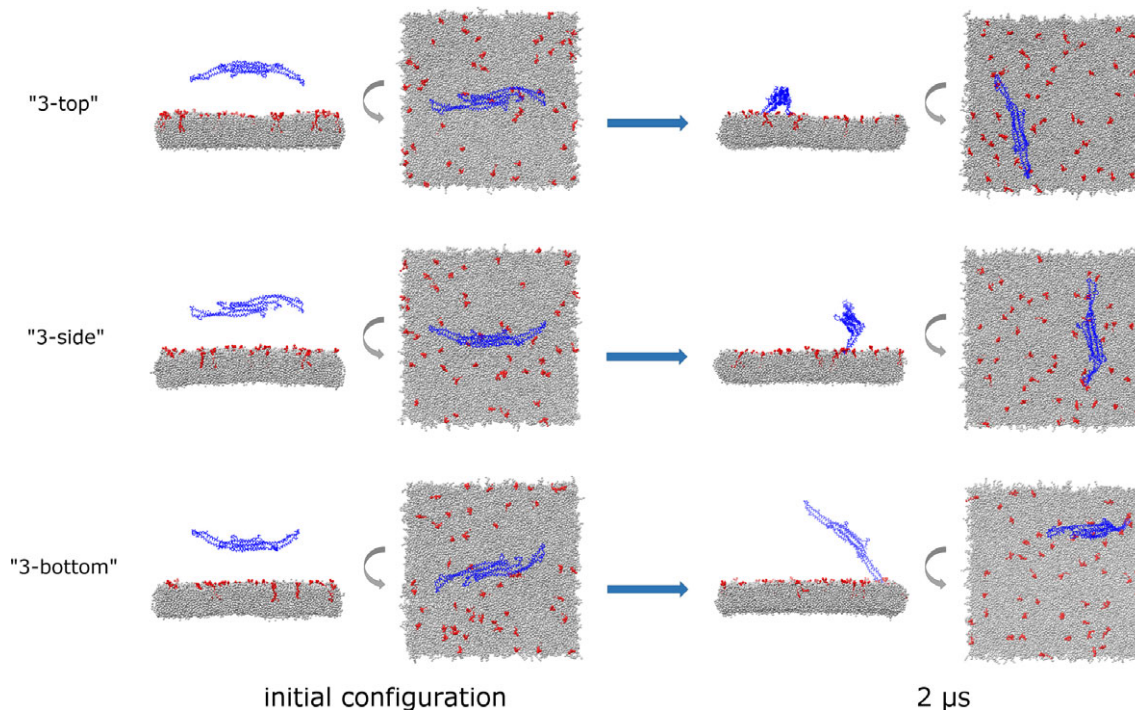


FIGURE 1 Simulation of systems with 3% DPPI concentration. Systems 3-top, 3-side, and 3-bottom after equilibration (left) and after 2 μ s of dynamics (right). DPPC lipids are colored in gray, DPPI lipids are red, the F-BAR domain is blue. BAR, Bin/Amphiphysin/Rvs; DPPC, dipalmitoyl phosphatidylcholine; DPPI, dipalmitoyl phosphatidylinositol 4,5-bisphosphate [Color figure can be viewed at wileyonlinelibrary.com]

command of GROMACS with the central part of the dimer in “top” orientation used as a reference for least square fitting. R_{zz} is the cosine of an angle between the z-axis of the protein, in the reference orientation, and the z-axis of the protein, at a given simulation time. Thus, R_{zz} values at the beginning of each simulation were 1, 0 and -1 for “top”, “side” and “bottom” systems, respectively. Prior to the *g_rotmat* calculation, the *trjconv* command was used to fit the rotation and translation of the protein in the xy plane. Two ensembles of $6 \times 2 \mu$ s and $6 \times 1.5 \mu$ s simulations were used to calculate histograms for 3% and 10% DPPI, respectively. For convergence analysis we also calculated density maps from $3 \times 1.5 \mu$ s ensembles for 10% DPPI (Supporting Information Figure S2, left) and from $3 \times 2 \mu$ s ensembles for 3% DPPI (Supporting Information Figure S2, right). Each histogram was normalized separately by its maximum value.

2D histograms have been built for DPPI distribution as a function of x and y coordinates of the membrane.

Plotting of the graphs was carried out in Octave.³³

2.6 | Electron microscopy of liposomes with bound Nwk

Liposome preparation and cryo-EM were described in Ref. 15. Briefly, liposomes were swelled from dried lipid films, in buffer containing 20 mM 4-(2-hydroxyethyl)-1-piperazineethanesulfonic acid, pH 7.5 and 100 mM NaCl. Liposomes were then extruded through a 200-nm filter (Avanti Polar Lipids, Alabaster, Alabama), and incubated with the purified Nwk for 30 minutes. Drops of the sample were applied to glow-discharged C-flat 1.2/1.3 copper 200 mesh grids (Protochips Inc., Raleigh, North Carolina) and plunge-frozen in liquid ethane. Cryo-specimens were loaded into a cooled Gatan cryoholder and recorded on a Tecnai F20

(FEI, Netherlands) transmission electron microscope (Brandeis Electron Microscopy Facility, Waltham, MA, USA) operated at 200 kV and equipped with a Gatan UltraScan 4000 4 k \times 4 k CCD camera (Gatan, CA). Images were taken at a nominal magnification of $\times 29\,000$, resulting in a pixel size of 3.74 Å. To analyze the cryo-images we used ImageJ program (<https://imagej.nih.gov/ij/index.html>). The density profiles (representative profiles are shown on Supporting Information Figure S6) were calculated across the membrane in deformed and non-deformed areas.

3 | RESULTS

3.1 | F-BAR membrane binding

In all simulations, the F-BAR diffused in the aqueous phase before making initial contact with PI(4,5)P₂ lipids (Figure 1). To track the process of membrane binding we calculated perpendicular distances between centers of mass of the protein and the lipid bilayer (Figure 2A). The graphs show that in all systems with 10% PI(4,5)P₂ the F-BAR domain was stably associated with the membrane by the end of the simulation. In systems with 3% DPPI, the protein either did not approach the membrane as closely or did not bind it as stably. Nevertheless, protein–lipid interactions were present in every simulation. The primary role in lipid binding was played by the F-BAR tips, which contain poly-lysine stretches (residues K178, K180, K181, K182, and K183). One of the tips was the first to encounter DPPI lipids and then stayed bound to the membrane for the rest of the run (Supporting Information Figure S3). At 10% DPPI, the second tip also approached the membrane, while at 3% DPPI, it was left in the aqueous phase in some systems. We tracked the trajectories of DPPI lipids,

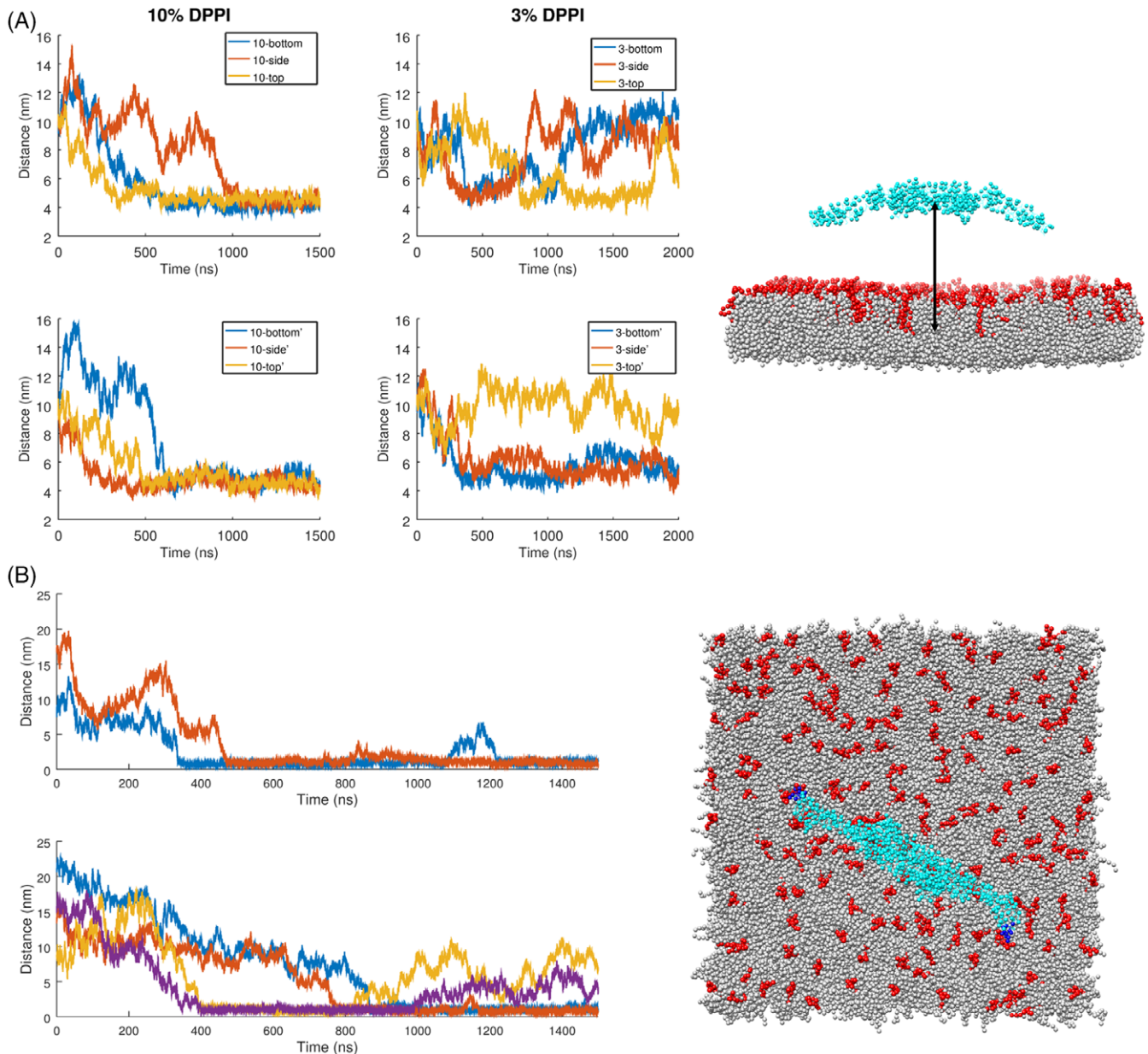


FIGURE 2 Binding of the F-BAR domain to membranes with different DPPI concentration. A, Perpendicular distances between the centers of mass of the F-BAR and the bilayer with 10% and 3% DPPI in the upper leaflet plotted as a function of time. Note that the name of a system only indicates the initial protein orientation which may change during the binding process. The 10-top system at the beginning of the simulation is shown on the right panel; the black arrow indicates the measured distance between the protein (cyan) and the membrane (gray DPPC and red DPPI). B, Distances between DPPI lipid headgroups and a dimer tip (residues 178-183) in 10-top system plotted as a function of time. Each curve corresponds to a single DPPI lipid: first tip interacted with two different DPPIs during the simulation, second tip interacted with four DPPIs. The right panel shows the 10-top system after 1.5 μ s simulation, residues 178-183 are colored in blue. BAR, Bin/Amphiphysin/Rvs; DPPC, dipalmitoyl phosphatidylcholine; DPPI, dipalmitoyl phosphatidylinositol 4,5-bisphosphate [Color figure can be viewed at wileyonlinelibrary.com]

which were in contact with lysine stretches in the 10-top system, and discovered that each tip was able to bind up to 2 DPPI molecules at the same time (Figure 2B). Electrostatic interactions between the lysine cluster and DPPI headgroups last for hundreds of nanoseconds.

To prove the validity of our models, we sought to compare lipid diffusion coefficients of the simulated membranes to the experimentally obtained data. To our knowledge, there are no experimental measurements of the PIP₂ diffusion coefficient in planar bilayers, in the presence of the F-BAR domain of Nwk. In this case, the DPPC diffusion coefficient may be used for validation of the model, as it has been extensively studied both computationally and experimentally. The values calculated

from our simulation were of the order of 1×10^{-7} cm²/s, which agrees well with the experimentally reported values for the DPPC bilayers at 321 K.³⁴ As expected, the DPPI lipids, in our systems, demonstrated an average of 20% lower values, due to interactions with the F-BAR. Thus, we concluded that our model membranes capture the lipid diffusion behavior well.

3.2 | Preferable orientation

To find out how DPPI concentration affects F-BAR domain membrane binding, we calculated 2D density maps of the relative protein

orientation and of the distance between the F-BAR domain and the bilayer. The density map for 10% DPPI shows two peaks: a higher one at R_{zz} values near 1 and a lower peak at R_{zz} near -1 (Figure 3, left side). When diffusing in water and making initial contacts with DPPI, the protein could rotate, but once it was bound to membrane, it adopted either a “top” or “bottom” orientation. The former was more probable and was observed in four out of six systems with 10% DPPI (Supporting Information Figure S4). A higher probability of the protein being bound to the membrane in “top” orientation may be due to a slightly higher number of DPPI lipids that could form contacts with it. For instance, in systems 10-top, 10-side, and 10-bottom, the average over the last 300 ns number of bound DPPIs was 9.9 ± 1.8 , 9.7 ± 1.6 , and 8.5 ± 1.4 , respectively. At 3% DPPI, the density is more diffusely distributed over the map with the highest peak at R_{zz} near 1 (Figure 3, right side). This may be explained by the fact that in some systems the F-BAR was interacting with lipids only by its tip and was staying at larger distances from the bilayer. This is in contrast with the 10% DPPI condition where the entire F-BAR was interacting with the membrane and did not rotate once it adopted the “top” or “bottom” position (Figure 2A and Supporting Information Figure S4).

3.3 | Amino acid residues interacting with PI(4,5)P₂

In order to determine which amino acid residues interact with the membrane, we calculated and normalized the frequency of contacts between each of the 288 residues and phosphate groups of DPPI lipids for all systems (Figure 4A and Supporting Information Figure S5).

The most frequent contacts were formed by residues at the F-BAR tips: poly-lysine stretch K178, K180, K181, K182, K183, and closely located K171, K173, K195, R199, R203, R204. Two other clusters with lower contact frequencies in 10% DPPI systems were located at the N-terminus (R6, K7, K12, K15) and the central part (K45, K59, K67, K68, K76). For 3% DPPI systems, residues from these two regions are also present on the diagram, although their frequencies are comparatively low. The higher ratio between tips and other residues at 3% DPPI concentration is due to the presence of “standing on the tip” states. Interestingly, this state also causes DPPI clustering at the site of tip binding (Figure 4B). This effect is less pronounced for 10% DPPI concentration due to a higher number of freely diffusing DPPIs, as well as protein-bound DPPIs.

4 | DISCUSSION

Here, we investigated membrane binding of the Nwk F-BAR domain using coarse-grained simulations. Comparison of protein binding to a membrane with different DPPI concentrations allowed us to describe differences in preferred orientation and identify residues involved in lipid binding. Our results indicate the importance of F-BAR dimer tips with poly-lysine stretches (K178, K180, K181, K182, K183). This motif is not highly conserved in mammalian homologs of Nwk, but it might play a role in the assembly of unique zigzag oligomers formed on the membrane by Nwk F-BAR domain dimers.¹³ The importance of dimer tips for membrane binding was previously established for a related F-BAR protein FBP17³⁵ and for I-BAR proteins: Pinkbar,³⁶ MIM⁴ and

IRSp53.³⁷ Interestingly, the stretch of lysines in Nwk is somewhat similar to a specific site in another membrane-binding and tubulating protein: GTPase MxA.³⁸ Single exchanges from lysine to glutamic acid in this protein resulted in disruption of co-sedimentation with liposomes. Our simulations suggest that a sequence with five lysines at the tips of the dimer of Nwk may play a similar role in lipid binding.

The microsecond-scale simulations allowed us to reveal different stages of the lipid binding process. In initial system configurations, the protein was located 7 nm above the membrane and we observed its rotation upon membrane binding. Thus, the initial F-BAR domain orientation did not dictate the binding orientation. Simultaneous binding of both tips is an unlikely event when F-BAR is diffusing in the aqueous phase before it finds the membrane. Instead, binding starts from one tip reaching the DPPI lipids while the rest of the dimer is left in solution. N-terminal residues (R6, K7, K12, K15) and the flexible loop between the first and the second α -helices (K67, K68, K76) may further attract the protein closer to the bilayer, eventually leading to residues in the central part of the concave surface (K45, K59) binding DPPI. The concentration of DPPI strongly affects the whole process. High DPPI levels result in strong electrostatic interactions, but the binding orientation may not be suitable for membrane-deforming activity. In systems with 10% DPPI, the protein was bound to membrane either by its concave surface (deformation-promoting mode) or by the opposite side (inactive; Figure 3). On the other hand, at low DPPI levels, the F-BAR domain is less attached to the membrane, in some cases being bound by only one tip, and thus is able to quickly change its relative orientation. As a result, the deformation-promoting mode becomes more favorable. Our data agree with previously conducted studies of F-BAR domain interactions with PI(4,5)P₂-containing liposomes which suggested that the F-BAR is biased toward a deformation-promoting orientation at low PI(4,5)P₂, while high PI(4,5)P₂ concentration leads to promiscuous binding and impedes liposome deformation.¹⁵ Indeed, high negative charge does not favor any possible orientation, but only two of them: with the concave surface facing the membrane (deformation-promoting) and by being rotated by 180° (inactive position). High negative charge also causes very stable membrane association, which may be inappropriate for the dynamic scaffold assembly and disassembly. Low negative charge, in contrast, allows the F-BAR to be membrane-associated, but at the same time able to change its position.

The role of N-terminal helices in membrane binding was described for N-BAR domains such as endophilin: EPR analysis was used to demonstrate that the amphipathic N-terminal region disordered in solution becomes arranged upon membrane binding and penetration.³⁹ The importance of the N-terminus for endophilin's *in vivo* functions was shown in *Caenorhabditis elegans*.⁴⁰ Membrane-binding properties of the N-termini of Nwk have not been studied experimentally yet, but we may speculate that, as flexible regions with positively charged residues, they may also take part in the membrane binding of the F-BAR domain.

An interesting feature observed in our simulations is a conformation, when the F-BAR was bound to membrane by only one tip (Figure 3 and Supporting Information Figure S3). This state was particularly stable at low DPPI concentration. In two systems with 3% DPPI, the protein first associated with the bilayer by two tips and the central part, but then dissociated from it leaving only one tip in contact with

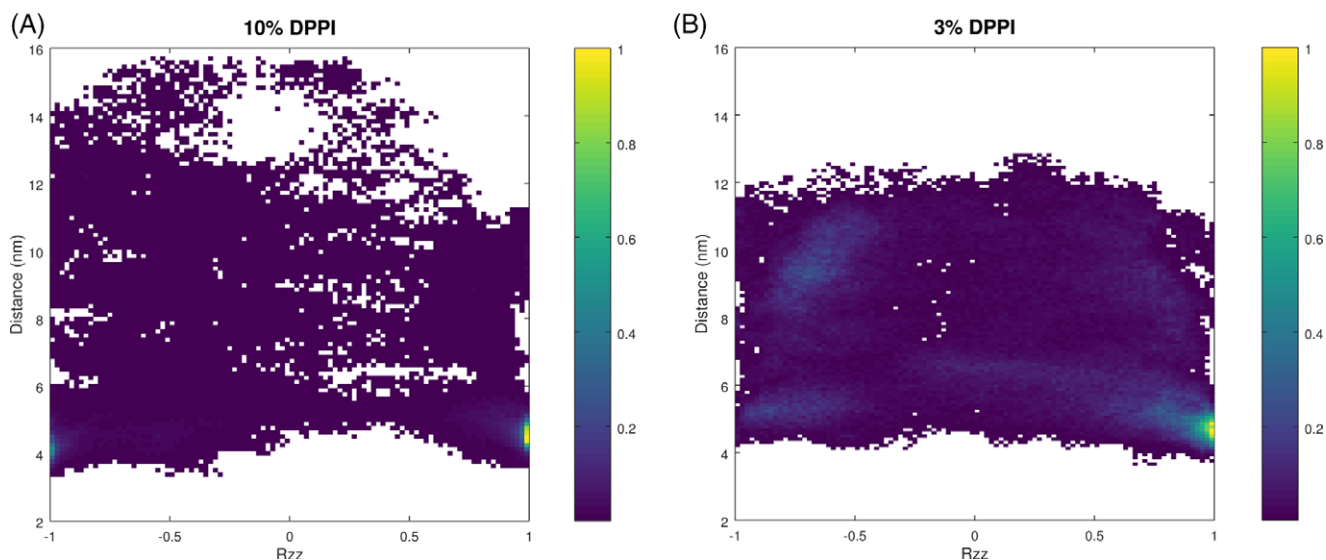


FIGURE 3 F-BAR domain binding to membranes. Normalized density maps for systems with 10% DPPI and 3% DPPI as functions of relative domain orientation R_{zz} and the perpendicular distance between the centers of mass of the protein and the bilayer. Each histogram was calculated from the ensemble of six simulations with corresponding DPPI concentration and normalized separately by its maximum value. BAR, Bin/Amphyphysin/Rvs; DPPI, dipalmitoyl phosphatidylinositol 4,5-bisphosphate [Color figure can be viewed at wileyonlinelibrary.com]

the lipids (Figure 2A and Supporting Information Figure S3, systems “3-top” and “3-side”). This is in agreement with cryo-EM analysis of liposome-bound Nwk. To demonstrate this, we reanalyzed images from

a previously reported dataset¹⁵ and found that in the area close to the membrane deformation, the Nwk molecules were mostly attached to the liposome with both tips, ready for the membrane deformation

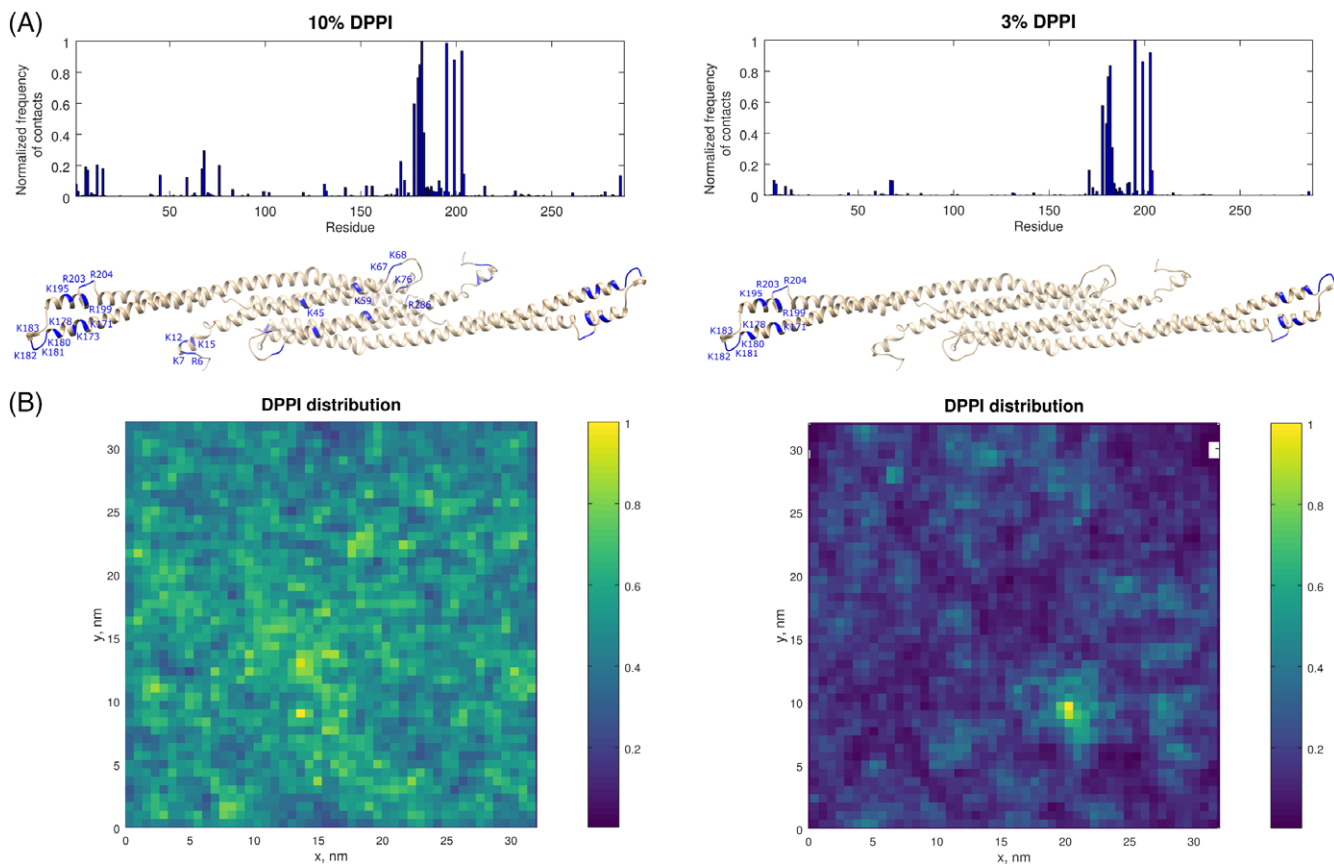


FIGURE 4 Amino acid residues in F-BAR interacting with DPPI lipids. A, Normalized frequency of contacts with DPPI lipids for systems with 10% and 3% DPPI (upper panel). Contacts were defined using the cut-off distance of 0.6 nm. The F-BAR dimer model as seen from the concave surface is shown on the lower panel; residues with the frequency of contacts ≥ 0.1 are colored blue and labeled in one monomer. B, Density maps for DPPI distribution in systems 10-top' and 3-side as functions of x and y coordinates of the membrane. Each histogram was calculated over the last 1 μ s of the simulation and normalized separately by its maximum value. BAR, Bin/Amphyphysin/Rvs; DPPI, dipalmitoyl phosphatidylinositol 4,5-bisphosphate [Color figure can be viewed at wileyonlinelibrary.com]

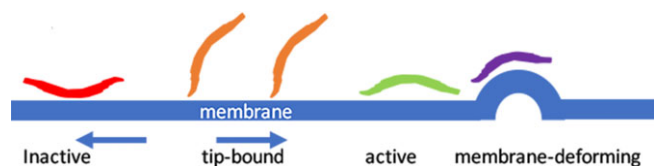


FIGURE 5 Dynamics of the F-BAR domain membrane-binding. Model of F-BAR membrane-binding, according to our molecular modeling study [Color figure can be viewed at wileyonlinelibrary.com]

(Supporting Information Figure S6). In the non-deformed area some Nwk interacted with the liposome with one tip, some interacted with its convex side down, and only few were positioned with the concave side toward the membrane.

We proposed that one tip bound conformation is necessary for the preliminary binding of the F-BAR to the liposome, quickly followed by either the upside down (inactive) conformation or by the anchoring of the second tip (active conformation) and, finally, membrane deformation (Figure 5). The one tip binding conformation may also simplify the protein–protein interactions at the beginning of the scaffold formation.

Altogether, our results suggest that membrane deforming is a multi-stage process, that includes the following steps: attracting the F-BAR to the membrane, one-tip membrane binding, interaction with neighboring F-BARs, both-tip membrane binding, and, finally, deforming of the membrane. Molecular dynamics of the assembly of multiple Nwk F-BAR domains on membranes with different lipid composition is yet to be explored.

ACKNOWLEDGMENTS

Authors thank Drs Avital Rodal and Daniela Nicastro for sharing the cryo-EM images of liposome-bound Nwk and Lisa Trifonova for proof-reading the manuscript. The reported study was funded by RFBR according to the research project No 18-34-00347. The research was carried out using the equipment of the shared research facilities of HPC computing resources at Lomonosov Moscow State University. No author declare the conflict of interest.

ORCID

Tatiana B. Stanishneva-Konvalova  <https://orcid.org/0000-0002-8427-8178>

Olga S. Sokolova  <https://orcid.org/0000-0003-4678-232X>

REFERENCES

- Peter BJ, Kent HM, Mills IG, et al. BAR domains as sensors of membrane curvature: the amphiphysin BAR structure. *Science*. 2004;303:495-499. <https://doi.org/10.1126/science.1092586>.
- Farsad K, Ringstad N, Takei K, Floyd SR, Rose K, De Camilli P. Generation of high curvature membranes mediated by direct endophilin bilayer interactions. *J Cell Biol*. 2001;155:193-200. <https://doi.org/10.1083/jcb.200107075>.
- Henne WM, Kent HM, Ford MGJ, et al. Structure and analysis of FCHo2 F-BAR domain: a dimerizing and membrane recruitment module that effects membrane curvature. *Structure*. 2007;15:839-852. <https://doi.org/10.1016/j.str.2007.05.002>.
- Mattila PK, Pykäläinen A, Saarikangas J, et al. Missing-in-metastasis and IRSp53 deform PI(4,5)P2-rich membranes by an inverse BAR domain-like mechanism. *J Cell Biol*. 2007;176:953-964. <https://doi.org/10.1083/jcb.200609176>.
- Zimmerberg J, McLaughlin S. Membrane curvature: how BAR domains bend bilayers. *Curr Biol*. 2004;14:250-252. <https://doi.org/10.1016/j.cub.2004.02.060>.
- Frost A, Perera R, Roux A, et al. Structural basis of membrane invagination by F-BAR domains. *Cell*. 2008;132:807-817. <https://doi.org/10.1016/j.cell.2007.12.041>.
- Zhao H, Michelot A, Koskela EV, et al. Membrane-sculpting BAR domains generate stable lipid microdomains. *Cell Rep*. 2013;4:1213-1223. <https://doi.org/10.1016/j.celrep.2013.08.024>.
- Picas L, Viaud J, Schauer K, et al. BIN1/M-Amphiphysin2 induces clustering of phosphoinositides to recruit its downstream partner dynamin. *Nat Commun*. 2014;5:5647. <https://doi.org/10.1038/ncomms6647>.
- McLaughlin S, Murray D. Plasma membrane phosphoinositide organization by protein electrostatics. *Nature*. 2005;438:605-611. <https://doi.org/10.1038/nature04398>.
- Coutinho-Budd J, Ghukasyan V, Zylka MJ, Polleux F. The F-BAR domains from srGAP1, srGAP2 and srGAP3 regulate membrane deformation differently. *J Cell Sci*. 2012;125:3390-3401. <https://doi.org/10.1242/jcs.098962>.
- Takeda T, Robinson IM, Savoian MM, et al. Drosophila F-BAR protein syndapin contributes to coupling the plasma membrane and contractile ring in cytokinesis. *Open Biol*. 2013;3:130081. <https://doi.org/10.1098/rsob.130081>.
- Stanishneva-Konvalova TB, Kelley CF, Eskin TL, et al. Coordinated autoinhibition of F-BAR domain membrane binding and WASp activation by nervous wreck. *Proc Natl Acad Sci*. 2016;113:E5552-E5561. <https://doi.org/10.1073/pnas.1524411113>.
- Becalska AN, Kelley CF, Berciu C, et al. Formation of membrane ridges and scallops by the F-BAR protein nervous wreck. *Mol Biol Cell*. 2013;24:2406-2418. <https://doi.org/10.1091/mbc.E13-05-0271>.
- Almeida-Souza L, Frank RAW, Garcia-Nafria J, et al. A flat BAR protein promotes actin polymerization at the base of clathrin-coated pits. *Cell*. 2018;174:325-337. <https://doi.org/10.1016/j.cell.2018.05.020>.
- Kelley CF, Messelaar EM, Eskin TL, Sokolova OS, Nicastro D, Rodal AA. Membrane charge directs the outcome of F-BAR domain lipid binding and autoregulation. *Cell Rep*. 2015;13:2597-2609. <https://doi.org/10.1016/j.celrep.2015.11.044>.
- Biasini M, Bienert S, Waterhouse A, et al. SWISS-MODEL: modelling protein tertiary and quaternary structure using evolutionary information. *Nucleic Acids Res*. 2014;42:252-258. <https://doi.org/10.1093/nar/gku340>.
- Thévenet P, Shen Y, Maupetit J, Guyon F, Derreumaux P, Tufféry P. PEP-FOLD: an updated de novo structure prediction server for both linear and disulfide bonded cyclic peptides. *Nucleic Acids Res*. 2012;40:288-293. <https://doi.org/10.1093/nar/gks419>.
- Pettersen EF, Goddard TD, Huang CC, et al. UCSF chimera—a visualization system for exploratory research and analysis. *J Comput Chem*. 2004;25:1605-1612. <https://doi.org/10.1002/jcc.20084>.
- De Jong DH, Singh G, Bennett WFD, et al. Improved parameters for the martini coarse-grained protein force field. *J Chem Theor Comput*. 2013;9:687-697. <https://doi.org/10.1021/ct300646g>.
- Periole X, Cavalli M, Marrink SJ, Ceruso MA. Combining an elastic network with a coarse-grained molecular force field: structure, dynamics, and intermolecular recognition. *J Chem Theor Comput*. 2009;5:2531-2543. <https://doi.org/10.1021/ct9002114>.
- Marrink SJ, Risselada HJ, Yefimov S, Tieleman DP, de Vries AH. The MARTINI force field: coarse grained model for biomolecular simulations. *J Phys Chem B*. 2007;111:7812-7824. <https://doi.org/10.1021/jp071097f>.
- López CA, Sovova Z, Van Eerden FJ, De Vries AH, Marrink SJ. Martini force field parameters for glycolipids. *J Chem Theor Comput*. 2013;9:1694-1708. <https://doi.org/10.1021/ct3009655>.
- Wassenaar TA, Ingólfsson HI, Böckmann RA, Tieleman DP, Marrink SJ. Computational lipidomics with insane: a versatile tool for generating custom membranes for molecular simulations. *J Chem Theor Comput*. 2015;11:2144-2155. <https://doi.org/10.1021/acs.jctc.5b00209>.

24. De Jong DH, Baoukina S, Ingólfsson HI, Marrink SJ. Martini straight: boosting performance using a shorter cutoff and GPUs. *Comput Phys Commun.* 2016;199:1-7. <https://doi.org/10.1016/j.cpc.2015.09.014>.
25. Essman U, Perera L, Berkowitz T, Darden T, Lee H, Pedersen LG. A smooth particle mesh Ewald method. *J Chem Phys.* 1995;103:8577-8593.
26. Bussi G, Donadio D, Parrinello M. Canonical sampling through velocity rescaling. *J Chem Phys.* 2007;126:014101. <https://doi.org/10.1063/1.2408420>.
27. Berendsen HJC, Postma JPM, van Gunsteren WF, DiNola A, Haak JR. Molecular dynamics with coupling to an external bath. *J Chem Phys.* 1984;81:3684-3690. <https://doi.org/10.1063/1.448118>.
28. Parrinello M, Rahman A. Polymorphic transitions in single crystals: a new molecular dynamics method. *J Appl Phys.* 1981;52:7182-7190.
29. Sadovnichy V, Tikhonravov A, Voevodin V, Opanasenko V. "Lomonosov": supercomputing at Moscow state university. In: Vetter JS, ed. *Contemporary High Performance Computation From Petascale Toward Exascale*. Boca Raton, FL: CRC Press; 2013:283-307. <https://doi.org/10.1201/b14677-14>.
30. Marrink SJ, de Vries AH, Mark AE. Coarse grained model for semi-quantitative lipid simulations. *J Phys Chem B.* 2004;108:750-760. <https://doi.org/10.1021/jp036508g>.
31. Blau C, Grubmuller H. g_contacts : fast contact search in bio-molecular ensemble data. *Comput Phys Commun.* 2013;184:2856-2859. <https://doi.org/10.1016/j.cpc.2013.07.018>.
32. Yamamoto E, Kalli AC, Yasuoka K, Sansom MSP. Interactions of Pleckstrin homology domains with membranes: adding Back the bilayer via high-throughput molecular dynamics. *Structure.* 2016;24:1421-1431. <https://doi.org/10.1016/j.str.2016.06.002>.
33. Eaton JW, Bateman D, Hauberg SÅ, Wehbring R. GNU Octave version 4.2.0 manual: a high-level interactive language for numerical computations. <http://www.gnu.org/software/octave/doc/interpreter/>. Accessed March 1, 2016.
34. Sheats JR, McConnell HM. A photochemical technique for measuring lateral diffusion of spin-labeled phospholipids in membranes. *Proc Natl Acad Sci USA.* 1978;75:4661-4663. <http://www.pubmedcentral.nih.gov/articlerender.fcgi?artid=336176&tool=pmcentrez&rendertype=abstract>.
35. Shimada A, Niwa H, Tsujita K, et al. Curved EFC/F-BAR-domain dimers are joined end to end into a filament for membrane invagination in endocytosis. *Cell.* 2007;129:761-772. <https://doi.org/10.1016/j.cell.2007.03.040>.
36. Pykäläinen A, Boczkowska M, Zhao H, et al. Pinkbar is an epithelial-specific BAR domain protein that generates planar membrane structures. *Nat Struct Mol Biol.* 2011;18:902-907. <https://doi.org/10.1038/nsmb.2079>.
37. Suetsugu S, Murayama K, Sakamoto A, et al. The RAC binding domain/IRSp53-MIM homology domain of IRSp53 induces RAC-dependent membrane deformation. *J Biol Chem.* 2006;281:35347-35358. <https://doi.org/10.1074/jbc.M606814200>.
38. Von Der Malsburg A, Abutbul-Ionita I, Haller O, Kochs G, Danino D. Stalk domain of the dynamin-like MxA GTPase protein mediates membrane binding and liposome tubulation via the unstructured L4 loop. *J Biol Chem.* 2011;286:37858-37865. <https://doi.org/10.1074/jbc.M111.249037>.
39. Gallop JL, Jao CC, Kent HM, et al. Mechanism of endophilin N-BAR domain-mediated membrane curvature. *EMBO J.* 2006;25:2898-2910. <https://doi.org/10.1038/sj.emboj.7601174>.
40. Schuske KR, Richmond JE, Matthies DS, et al. Endophilin is required for synaptic vesicle endocytosis by localizing synaptojanin. *Neuron.* 2003;40:749-762. [https://doi.org/10.1016/S0896-6273\(03\)00667-6](https://doi.org/10.1016/S0896-6273(03)00667-6).

SUPPORTING INFORMATION

Additional supporting information may be found online in the Supporting Information section at the end of this article.

How to cite this article: Stanishneva-Konovalova TB, Sokolova OS. Effects of PI(4,5)P₂ concentration on the F-BAR domain membrane binding as revealed by coarse-grained simulations. *Proteins.* 2019;1-8. <https://doi.org/10.1002/prot.25678>